




PAPER

[View Article Online](#)
[View Journal](#) | [View Issue](#)Cite this: *Dalton Trans.*, 2024, **53**,
5453Introducing sterically demanding substituents and π - π -interactions into $[\text{Cu}(\text{P}^{\wedge}\text{P})(\text{N}^{\wedge}\text{N})]^+$ complexes†Marco Meyer,  Alessandro Prescimone,  Edwin C. Constable  and
Catherine E. Housecroft *

A series of ten $\text{N}^{\wedge}\text{N}$ chelating ligands based on a 2,2'-bipyridine (bpy) metal-binding domain and featuring sterically hindering substituents in the 6- and 6,6'-positions has been synthesized and characterized. The ligands have been incorporated into a family of 15 heteroleptic complexes of type $[\text{Cu}(\text{P}^{\wedge}\text{P})(\text{N}^{\wedge}\text{N})][\text{PF}_6]$ where $\text{P}^{\wedge}\text{P}$ is the wide bite-angle bisphosphane ligand bis(2(diphenylphosphanyl)phenyl)ether (POP) or (9,9-dimethyl-9H-xanthene-4,5-diyl)bis(diphenylphosphane) (xantphos). Substituents in several of the $\text{N}^{\wedge}\text{N}$ ligands possess phenyl rings remotely tethered to enable intra- and intermolecular π - π -interactions in the $[\text{Cu}(\text{P}^{\wedge}\text{P})(\text{N}^{\wedge}\text{N})]^+$ cations. Single crystal X-ray structures of 12 complexes are reported. The effects of the functional groups in the bpy ligand on the photophysical properties of the complexes have been studied; solid-state emission maxima range from 518 to 567 nm. Values of the solid-state photoluminescence quantum yields (PLQYs) of the $[\text{Cu}(\text{P}^{\wedge}\text{P})(\text{N}^{\wedge}\text{N})][\text{PF}_6]$ compounds respond to the nature of the $\text{N}^{\wedge}\text{N}$ ligand. In general, we observed that the $[\text{Cu}(\text{P}^{\wedge}\text{P})(\text{N}^{\wedge}\text{N})]^+$ complexes containing 6,6'-disubstituted complexes with phenyl moieties connected via a CH_2CH_2 or $\text{CH}_2\text{CH}_2\text{CH}_2$ spacer to the bpy domain have the highest values of PLQY. The most significant compounds are $[\text{Cu}(\text{POP})((2\text{-PhEt})_2\text{bpy})][\text{PF}_6]$ (PLQY = 67%) and $[\text{Cu}(\text{POP})((3\text{-PhPr})_2\text{bpy})][\text{PF}_6]$ (PLQY = 72%) where $(2\text{-PhEt})_2\text{bpy}$ = 6,6'-bis(2-phenylethyl)-2,2'-bipyridine and $(3\text{-PhPr})_2\text{bpy}$ = 6,6'-bis(3-phenylpropyl)-2,2'-bipyridine. These PLQY values are among the best performing previously reported families of $[\text{Cu}(\text{P}^{\wedge}\text{P})(\text{N}^{\wedge}\text{N})][\text{PF}_6]$ compounds.

Received 30th January 2024,
Accepted 19th February 2024

DOI: 10.1039/d4dt00276h

rsc.li/dalton

Introduction

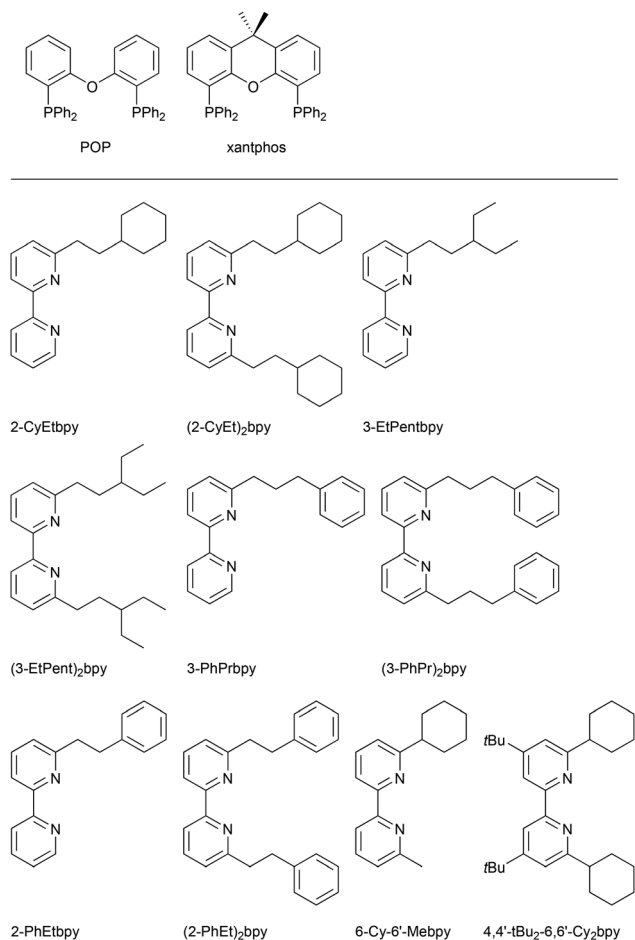
A noteworthy property of certain families of copper(i) based coordination compounds is that they can exhibit thermally activated delayed fluorescence (TADF), enabling enhanced photoluminescence quantum yields (PLQYs).^{1–7} Copper(i) complexes of the type $[\text{Cu}(\text{P}^{\wedge}\text{P})(\text{N}^{\wedge}\text{N})]^+$ ($\text{N}^{\wedge}\text{N}$ = chelating diimine ligand and $\text{P}^{\wedge}\text{P}$ = bidentate bis(phosphane) ligand) are of interest for use in light-emitting electrochemical cells (LECs).⁶ McMillin *et al.* first reported the photoluminescence of $[\text{Cu}(\text{PPh}_3)_2(\text{bpy})]^+$ complexes (bpy = 2,2'-bipyridine) following a metal-to-ligand charge-transfer (MLCT) excitation⁸ with subsequent studies employing $[\text{Cu}(\text{N}^{\wedge}\text{N})_2]^+$ and $[\text{Cu}(\text{P}^{\wedge}\text{P})(\text{N}^{\wedge}\text{N})]^+$

emitters.^{9–13} To enhance the photophysical properties of the $[\text{Cu}(\text{P}^{\wedge}\text{P})(\text{N}^{\wedge}\text{N})]^+$ coordination compounds,^{3,6} wide-angle bisphosphane ligands such as xantphos or POP (Scheme 1) are often employed as the $\text{P}^{\wedge}\text{P}$ ligand.¹⁴ The presence of intramolecular π -stacking interactions between arene rings is beneficial to the PLQY values of the complexes.^{6,15}

For improved chemical stability and beneficial photophysical properties, the stabilization of the tetrahedral coordination geometry of the copper(i) centre is an essential feature in $[\text{Cu}(\text{P}^{\wedge}\text{P})(\text{N}^{\wedge}\text{N})]^+$ species.^{6,16,17} When such compounds are employed in the emitting layers of LEC devices, the use of small alkyl substituents such as methyl and ethyl in the 6- or 6,6'-positions of the bpy ligand backbone enhance LEC performances.¹⁸ The desymmetrization of the $\text{N}^{\wedge}\text{N}$ ligand with a phenyl substituent in the 6-position gave rise to interesting structural properties of the complex cations. In $[\text{Cu}(\text{xantphos})(\text{Phbpy})]^+$ cations (Phbpy = 6-phenyl-2,2'-bipyridine), the phenyl group of the Phbpy was not accommodated in the xanthene 'bowl' of the xantphos ligand but the ligand was instead flipped by 180°. If the tetrahedral coordination sphere around the Cu(i) centre is not sterically protected, flattening towards a square-planar geometry can occur after MLCT photoexcitation. This geometry permits close contact of

Department of Chemistry, University of Basel, Mattenstrasse 24a, BPR 1096,
4058 Basel, Switzerland. E-mail: catherine.housecroft@unibas.ch

† Electronic supplementary information (ESI) available: Experimental details and analytical data for the copper(i) compounds; Fig. S2–S127: ¹H, HMQC and HMBC NMR spectra, mass spectra, FTIR spectra and UV-Vis spectra; Table S1: Crystallographic data; Fig. S128–140: Structural figures; Fig. S141–S142: Cyclic voltammograms; Fig. S143: Photographs of powdered samples of $[\text{Cu}(\text{POP})(\text{N}^{\wedge}\text{N})][\text{PF}_6]$ complexes. CCDC 2324342–2324349, 2324365–2324369. For ESI and crystallographic data in CIF or other electronic format see DOI: <https://doi.org/10.1039/d4dt00276h>



Scheme 1 Top: structures of the POP and xantphos P[^]P ligands. Bottom: structures and abbreviations of the N[^]N ligands.

the centre with solvent and other surrounding molecules and ions, potentially forming 5-coordinate exciplexes and emission quenching. It has also been shown that intramolecular π -stacking interactions in $[\text{Cu}(\text{P}^{\wedge}\text{P})(\text{phen})]^+$ and $[\text{Cu}(\text{P}^{\wedge}\text{P})(4,7\text{-Ph}_2\text{phen})]^+$ (4,7- Ph_2phen = 4,7-diphenyl-1,10-phenanthroline) lead to increased PLQY values because of inhibition of the flattening of the coordination sphere in the excited state.¹⁵ Additional studies reveal that introducing 6-phenylthio substituents to the bpy domain is beneficial to the photophysical properties of $[\text{Cu}(\text{POP})(\text{bpy})]^+$ and $[\text{Cu}(\text{xantphos})(\text{bpy})]^+$ salts.^{18–20}

The photophysical properties of $[\text{Cu}(\text{P}^{\wedge}\text{P})(\text{N}^{\wedge}\text{N})]^+$ complexes can be improved by structural modification of either the P[^]P or the N[^]N domains. The most popular choice for the P[^]P ligand is a wide bite-angle bisphosphane such as POP or xantphos, which are commercially available, well documented in the literature, and have established structure–property relationships.^{21–23} However, enhancing PLQY at the same time as improving the performance of the complexes in a LEC environment is only possible through trial-and-error structural variation of the P[^]P and N[^]N ligands. Detailed density functional theory (DFT) calculations have been carried out on a

number of series of $[\text{Cu}(\text{P}^{\wedge}\text{P})(\text{N}^{\wedge}\text{N})]^+$ complexes and probe the nature of the low lying electronic states, as well as the energy difference between the different conformers of $[\text{Cu}(\text{xantphos})(6\text{-Rbpy})]^+$ cations.^{18,20}

Another challenge in the design of $[\text{Cu}(\text{P}^{\wedge}\text{P})(\text{N}^{\wedge}\text{N})]^+$ emitters is to minimize the tendency for ligand-redistribution reactions. One approach has been to use macrocyclic ligands to produce pseudorotaxanes.^{4,24} The introduction of sterically demanding substituents within the coordination sphere of the copper(i) centre is one of the simplest strategies for limiting ligand-redistributions. In this work, we focus on the modification of the N[^]N ligand, this being synthetically more facile than functionalization of the P[^]P domain. The aim was to introduce sterically demanding substituents in the 6- and 6,6'-positions of the bpy ligand in $[\text{Cu}(\text{POP})(\text{bpy})]^+$ and $[\text{Cu}(\text{xantphos})(\text{bpy})]^+$ and to investigate the solution dynamic behaviour of the complexes as well as their solid-state structures and electrochemical and photophysical properties. However, to the best of our knowledge, little is known about the effects of introducing longer and potentially sterically demanding 6- and 6,6'-substituents. Although there are limitations to the steric bulk of 6- and 6,6'-substituents that can be accommodated within the coordination sphere of the copper(i) centre, the recent work of Wöhler *et al.*⁴ demonstrated that heteroleptic $[\text{Cu}(\text{POP})(\text{N}^{\wedge}\text{N})]^+$ and $[\text{Cu}(\text{xantphos})(\text{N}^{\wedge}\text{N})]^+$ complexes containing 6,6'-bis(but-3-en-1-yl)-2,2'-bipyridine, 6-(but-3-en-1-yl)-6'-methyl-2,2'-bipyridine, 6,6'-bis(pent-4-en-1-yl)-2,2'-bipyridine and 6-(pent-4-en-1-yl)-6'-methyl-2,2'-bipyridine could be prepared and were stable with respect to ligand dissociation in solution. We were therefore motivated to explore the use of long-chain substituents of having similar steric requirements to those of Wöhler *et al.* but also incorporating terminal phenyl groups with the potential for π -stacking interactions. The range of ligands chosen is shown in Scheme 1.

Experimental

General

Reactions under microwave conditions were carried out in a Biotage Initiator+ microwave reactor. ¹H, ¹³C{¹H}, ¹⁹F{¹H} and ³¹P{¹H} NMR spectra were recorded at *ca.* 295 K in acetone-*d*₆ or CDCl₃ using a Bruker Avance III-500 NMR spectrometer. ¹H and ¹³C chemical shifts were referenced to residual solvent peaks (¹H $\delta(\text{acetone-}d_3) = 2.50$ ppm, ¹³C $\delta(\text{acetone-}d_6) = 29.84$ ppm). Absorption and emission spectra in solution were measured using a Shimadzu UV-2600 spectrophotometer and a Shimadzu RF-5301-PC spectrofluorometer, respectively. A Shimadzu LCMS-2020 instrument was used to record electrospray (ESI) mass spectra. spectrophotometer. MALDI mass spectra were measured using a Shimadzu MALDI-8020 instrument with α -cyano-4-hydroxycinnamic acid solution as matrix for sample preparation.

Quantum yields (CH_2Cl_2 solution and powder) were measured using a Hamamatsu absolute photoluminescence (PL) quantum yield spectrometer C11347 Quantaury-QY.



Powder emission spectra and excited state lifetimes were measured with a Hamamatsu Compact Fluorescence lifetime Spectrometer C11367 Quantaurs-Tau using an LED light source ($\lambda_{\text{exc}} = 365 \text{ nm}$). Lifetimes were obtained by fitting the measured data to an exponential decay using MATLAB®; a biexponential fit was used when a single exponential fit gave a poor fit. Where stated, the sample was degassed using argon bubbling for 20 min.

Electrochemical measurements were performed using an Ametek VersaSTAT 3F potentiostat with $[\text{Bu}_4\text{N}][\text{PF}_6]$ (0.1 M) as supporting electrolyte and a scan rate of 0.1 V s^{-1} ; the solvent was dry 4-methyl-1,3-dioxolan-2-one carbonate and solution concentrations were $\text{ca. } 2 \times 10^{-3} \text{ mol dm}^{-3}$. The solutions were constantly degassed with argon. The working electrode was glassy carbon, the reference electrode was a leakless Ag/AgCl (eDAQ ET069-1, electrolyte aqueous KCl, conc. 3.4 mol dm^{-3}) and the counter-electrode was a platinum wire. Final potentials were internally referenced with respect to an Fc/Fc⁺ couple.

$[\text{Cu}(\text{MeCN})_4][\text{PF}_6]$ was prepared according to the literature procedure.²⁵ Diisopropylamine, *n*-butyllithium in hexanes, 1-bromo-4-phenylbutane, (bromomethyl)-cyclohexane, 1-bromo-2-ethylbutane, benzyl bromide, (2-bromoethyl)-benzene, trifluoroacetic acid, di-*tert*-butyl peroxide, 2,3-butanedione, 4,4'-bis(bromomethyl)-2,2'-bipyridine, POP and xantphos were purchased from Acros Organics. 2-Chloro-6-methylpyridine was bought from Apollo Scientific, 6,6'-dimethyl-2,2'-bipyridine (Me_2bpy) from Fluorochem and $[\text{Pd}(\text{PPh}_3)_4]$ from Sigma Aldrich. 6-Methyl-2,2'-bipyridine (Mebpy) was prepared by a Negishi coupling reaction following a microwave reactor adaption²⁶ of a literature method described by Kim *et al.*²⁷ The NMR spectroscopic data of the compounds prepared after literature methods were consistent with those reported.

Syntheses and characterization of N^N ligands and copper(I) compounds

General procedures for ligand syntheses were adapted from the literature.^{28,29} Details of syntheses, ^1H , $^{13}\text{C}\{^1\text{H}\}$, $^{19}\text{F}\{^1\text{H}\}$, and $^{31}\text{P}\{^1\text{H}\}$ NMR characterization and assignments, MALDI/electrospray mass spectrometric data, FTIR spectra, UV-Vis spectra and elemental analyses are given in the ESI.†

Crystallography

Crystallographic data for all the compounds are presented in Table S1.† Single crystal data were collected on a Bruker APEX-II diffractometer (CuK α radiation, see Table S1†) with data reduction, solution and refinement using the programs APEX,³⁰ ShelXT,³¹ Olex2,³² and ShelXL v. 2014/7,³³ or using a STOE StadiVari diffractometer equipped with a Pilatus300K detector and with a Metaljet D2 source (GaK α radiation) or on a STOE StadiVari diffractometer equipped with a Eiger2 1 M detector (CuK α radiation) or on a Rigaku XtaLAB Mini II diffractometer with an Hybrid Pixel Array Detector (MoK α radiation) (see Table S1†) and solving the structure using Superflip,^{34,35} and Olex2.³² The structural model was refined with ShelXL v. 2014/7.³³ Structure analysis used Mercury CSD

v. 2021.1.0.³⁶ In $[\text{Cu}(\text{xantphos})(2\text{-CyEtbp})][\text{PF}_6] \cdot 1.5\text{Et}_2\text{O}$, a solvent mask was used to treat the solvent region and all of the formulae and numbers were appropriately modified. In $[\text{Cu}(\text{POP})(3\text{-EtPentbp})][\text{PF}_6]$ (polymorph 1), the solvent mask was used to treat the solvent region: half a CH_2Cl_2 molecule was found per unit and added to all of the formulae and numbers. With $[\text{Cu}(\text{POP})((2\text{-PhEt})_2\text{bpy})][\text{PF}_6] \cdot 1.125\text{Et}_2\text{O}$, a solvent mask was used to treat part of the solvent region; all of the numbers and formulae take this into account. In $[\text{Cu}(\text{xantphos})(3\text{-PhPrbp})][\text{PF}_6] \cdot 0.8\text{Et}_2\text{O}$, a solvent mask was again used to treat the solvent region; the aromatic ring on the bpy arm is disordered over 2 orientations with fractional occupancies 0.65 and 0.35. In $[\text{Cu}(\text{xantphos})(6\text{-Cy-6'-Mebpy})][\text{PF}_6] \cdot 0.75\text{Et}_2\text{O} \cdot 0.5\text{H}_2\text{O}$, the solvent region is heavily disordered and restraints were applied. In $[\text{Cu}((2\text{-CyEt})_2\text{bpy})_2][\text{PF}_6]$, one cyclohexyl moiety is disordered over two sites with site occupancies of 65% and 35%, respectively.

Results and discussion

Synthesis of the N^N ligands

For the ligand synthesis, two different pathways were followed and are summarized in Schemes 3 and 4. The first procedure (Scheme 3) involved structural elucidation of an existing alkyl substituent and were adapted from a literature procedure.²⁸ The first step was lithiation of the methyl groups in 6-methyl-2,2'-bipyridine (Mebpy) or 6,6'-dimethyl-2,2'-bipyridine (Me_2bpy) using which lithium diisopropylamide (LDA). The intermediate was then treated with the desired bromoalkane to give the 6- or 6,6'-functionalized bpy in yields ranging between 30–57% after purification by column chromatography. The bromoalkane was added in 0.85 or 1.70 equivalents respectively for the singly and doubly substituted ligands minimizing side products.

The second procedure (Scheme 4) was used to functionalize bpy with directly connected cyclohexyl groups. A previously published metal-free cross-dehydrogenative coupling reaction (photocatalysed cross-dehydrogenative Minisci alkylation) was used.²⁹ The reaction uses butane-2,3-dione as a photosensitizer and di-*tert*-butyl peroxide as a radical initiator. According to the reported ketone-enabled mechanism, both butane-2,3-dione and the excited di-*tert*-butyl peroxide molecules can act as hydrogen abstractors to generate alkyl radicals from cyclohexane.²⁹ As these react with the heteroarene rings of the bpy, a hydrogen radical is trapped from the coupling product by the two free radical species formed in the hydrogen abstraction step. This affords the target compounds. The target compounds were obtained in low yields (12% for 4,4'-di-*tert*-butyl-6,6'-dicyclohexyl-2,2'-bipyridine and 18% for 6-cyclohexyl-6'-methyl-2,2'-bipyridine).

The ligands were characterized by ^1H and $^{13}\text{C}\{^1\text{H}\}$ NMR, IR and absorption spectroscopies and mass spectra, and data are presented in the Experimental section and Fig. S1–S62 in the ESI.†



Synthesis of the $[\text{Cu}(\text{P}^{\wedge}\text{P})(\text{N}^{\wedge}\text{N})][\text{PF}_6]$ complexes

Two different strategies were followed to prepare the complexes containing POP and xantphos respectively. For $[\text{Cu}(\text{POP})(\text{N}^{\wedge}\text{N})][\text{PF}_6]$, a sequential ligand addition pathway was followed, whereas for $[\text{Cu}(\text{xantphos})(\text{N}^{\wedge}\text{N})][\text{PF}_6]$, the ligands were added simultaneously to $[\text{Cu}(\text{MeCN})_4][\text{PF}_6]$. The reasons for these different approaches have been discussed in detail previously.^{18,37}

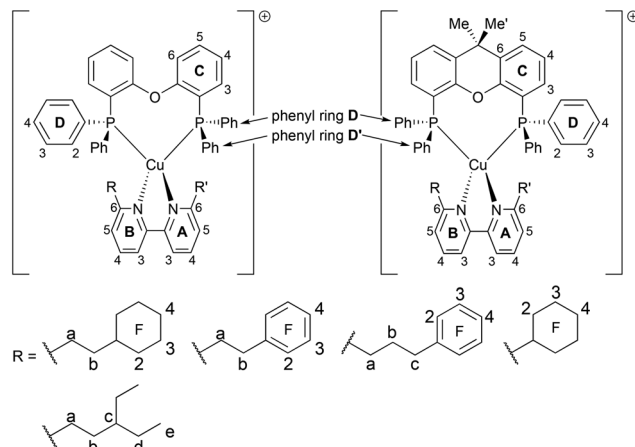
The detailed conditions and purification methods are given in the Experimental section in ESI.† The $[\text{Cu}(\text{P}^{\wedge}\text{P})(\text{N}^{\wedge}\text{N})][\text{PF}_6]$ complexes were obtained as yellow solids in yields of 56–81% after purification. We note that the attempted syntheses of $[\text{Cu}(\text{POP})((2\text{-CyEt})_2\text{bpy})][\text{PF}_6]$, $[\text{Cu}(\text{xantphos})((2\text{-CyEt})_2\text{bpy})][\text{PF}_6]$, $[\text{Cu}(\text{POP})((3\text{-EtPent})_2\text{bpy})][\text{PF}_6]$, $[\text{Cu}(\text{xantphos})((3\text{-EtPent})_2\text{bpy})][\text{PF}_6]$, $[\text{Cu}(\text{POP})(4,4'\text{-tBu}_2\text{-6,6'-Cy}_2\text{bpy})][\text{PF}_6]$, $[\text{Cu}(\text{xantphos})(4,4'\text{-tBu}_2\text{-6,6'-Cy}_2\text{bpy})][\text{PF}_6]$ and $[\text{Cu}(\text{POP})(6\text{-Cy-6'-Mebpy})][\text{PF}_6]$ were unsuccessful, presumably because of severe steric hindrance. For these $\text{N}^{\wedge}\text{N}$ ligands, the close proximity of the bulky 6,6'-substituents apparently hinders the coordination of the $\text{P}^{\wedge}\text{P}$ ligands rendering the heteroleptic complexes unstable in solution. Instead of the desired heteroleptic $[\text{Cu}(\text{P}^{\wedge}\text{P})(\text{N}^{\wedge}\text{N})][\text{PF}_6]$ complexes, a poorly defined mixture of complexes was obtained, including the homoleptic complex $[\text{Cu}(\text{N}^{\wedge}\text{N})_2][\text{PF}_6]$ in combination with $[\text{Cu}(\text{xantphos})_2][\text{PF}_6]$ or $[\text{Cu}(\text{POP})(\text{MeCN})][\text{PF}_6]$ and $[\text{Cu}(\text{POP-P,P})(\text{POP-P})][\text{PF}_6]$. These conclusions were based on the ^1H and $^{31}\text{P}\{^1\text{H}\}$ NMR spectra of the mixtures of products in addition to mass spectrometric data. Red crystals obtained from the attempted syntheses of $[\text{Cu}(\text{POP})((2\text{-CyEt})_2\text{bpy})][\text{PF}_6]$ and $[\text{Cu}(\text{xantphos})((2\text{-CyEt})_2\text{bpy})][\text{PF}_6]$ proved to be $[\text{Cu}((2\text{-CyEt})_2\text{bpy})_2][\text{PF}_6]$, the structure of which is described later.

Characterization of the copper(i) complexes

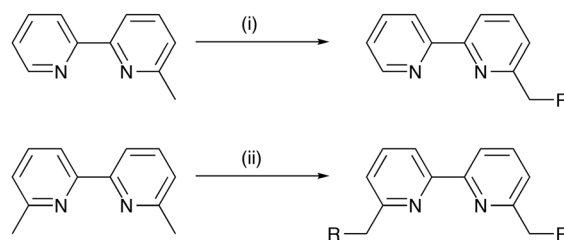
The positive mode electrospray mass spectrum of each compound exhibited peak envelopes arising from the $[\text{Cu}(\text{POP})(\text{N}^{\wedge}\text{N})]^+$ or $[\text{Cu}(\text{xantphos})(\text{N}^{\wedge}\text{N})]^+$ cations as well as from the $[\text{Cu}(\text{POP})]^+$ or $[\text{Cu}(\text{xantphos})]^+$ cation (see Experimental section in ESI†). ^1H , $^{13}\text{C}\{^1\text{H}\}$, $^{19}\text{F}\{^1\text{H}\}$ and $^{31}\text{P}\{^1\text{H}\}$ NMR spectra were recorded at room temperature in acetone- d_6 or CDCl_3 solutions. The ^1H and $^{13}\text{C}\{^1\text{H}\}$ spectra were assigned using COSY, NOESY, HMQC and HMBC techniques; atom labelling used for NMR assignments are given in Scheme 2. Fig. 1 shows the aromatic regions of the ^1H NMR spectra of $[\text{Cu}(\text{POP})(3)][\text{PF}_6]$, $[\text{Cu}(\text{xantphos})(3\text{PhPrbpy})][\text{PF}_6]$, $[\text{Cu}(\text{xantphos})((3)_2\text{bpy})][\text{PF}_6]$ and $[\text{Cu}(\text{POP})((3)_2\text{bpy})][\text{PF}_6]$ as representative examples (see Fig. S63–S127† for ^1H , HMQC and HMBC NMR, ESI-MS and FTIR spectra of all the complexes).

Single crystal structures

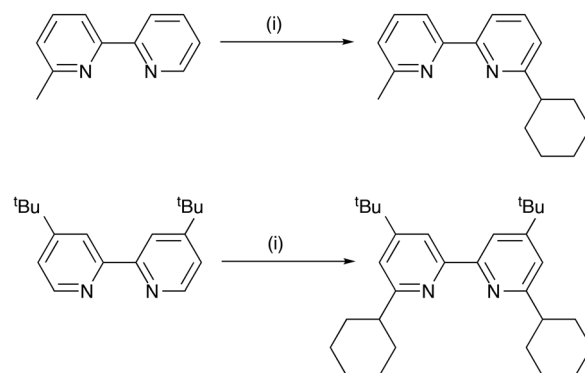
X-ray quality single crystals of $[\text{Cu}(\text{xantphos})(2\text{-CyEtbpy})][\text{PF}_6] \cdot 1.5\text{Et}_2\text{O}$, $[\text{Cu}(\text{POP})(3\text{-EtPentbpy})][\text{PF}_6]$ (polymorph 1), $[\text{Cu}(\text{POP})(3\text{-EtPentbpy})][\text{PF}_6]$ (polymorph 2), $[\text{Cu}(\text{xantphos})(3\text{-EtPentbpy})][\text{PF}_6] \cdot 0.8\text{Et}_2\text{O}$, $[\text{Cu}(\text{POP})(2\text{-PhEtbpy})][\text{PF}_6] \cdot 0.4\text{CH}_2\text{Cl}_2 \cdot 0.75\text{Et}_2\text{O}$, $[\text{Cu}(\text{xantphos})(2\text{-PhEtbpy})][\text{PF}_6] \cdot 0.5\text{Et}_2\text{O}$, $[\text{Cu}(\text{POP})((2\text{-PhEt})_2\text{bpy})][\text{PF}_6] \cdot 1.125\text{Et}_2\text{O}$, $[\text{Cu}(\text{xantphos})((2\text{-PhEt})_2\text{bpy})][\text{PF}_6] \cdot 1.125\text{Et}_2\text{O}$, $[\text{Cu}(\text{xantphos})(6\text{-Cy-6'-Mebpy})][\text{PF}_6] \cdot 0.75\text{Et}_2\text{O} \cdot 0.5\text{H}_2\text{O}$



Scheme 2 Structures of the $[\text{Cu}(\text{POP})(\text{N}^{\wedge}\text{N})]^+$ and $[\text{Cu}(\text{xantphos})(\text{N}^{\wedge}\text{N})]^+$ cations with ring and atom labelling for NMR spectroscopic data. When $\text{R} = \text{H}$, the rings are labelled A and B as shown. When $\text{R} = \text{R}'$, the pyridine rings are equivalent and are labelled B. Non-backbone phenyl rings in the $\text{P}^{\wedge}\text{P}$ ligands are labelled D. The rings on the substituents R (connected via chains to the bpy ligand), are labelled F.



Scheme 3 Reaction scheme for the first general procedure for ligand synthesis. Conditions: (i) $n\text{-BuLi}$ (1 equiv.), LDA (1 equiv.), RBr (0.85 equiv.); THF/hexane; $-78\text{ }^\circ\text{C}$; 8 h; (ii) $n\text{-BuLi}$ (2 equiv.), LDA (2 equiv.), RBr (1.7 equiv.); THF/hexane; $-78\text{ }^\circ\text{C}$; 8 h.



Scheme 4 Reaction scheme for the second general procedure for ligand synthesis. Conditions: (i) cyclohexane; trifluoroacetic acid (2 equiv.), di-*tert*-butyl peroxide (8 equiv.), butane-2,3-dione (23 equiv.); MeCN; 295 K, 7 days, irradiation 470 nm.

$[\text{Cu}(\text{POP})(3\text{-PhPrbpy})][\text{PF}_6]$, $[\text{Cu}(\text{POP})(3\text{-PhPrbpy})][\text{PF}_6]$, $[\text{Cu}(\text{xantphos})(3\text{-PhPrbpy})][\text{PF}_6] \cdot 0.8\text{Et}_2\text{O}$, $[\text{Cu}(\text{POP})((3\text{-PhPr})_2\text{bpy})][\text{PF}_6] \cdot 0.5\text{CH}_2\text{Cl}_2 \cdot 0.5\text{Et}_2\text{O}$, $[\text{Cu}(\text{xantphos})(6\text{-Cy-6'-Mebpy})][\text{PF}_6] \cdot 0.75\text{Et}_2\text{O} \cdot 0.5\text{H}_2\text{O}$



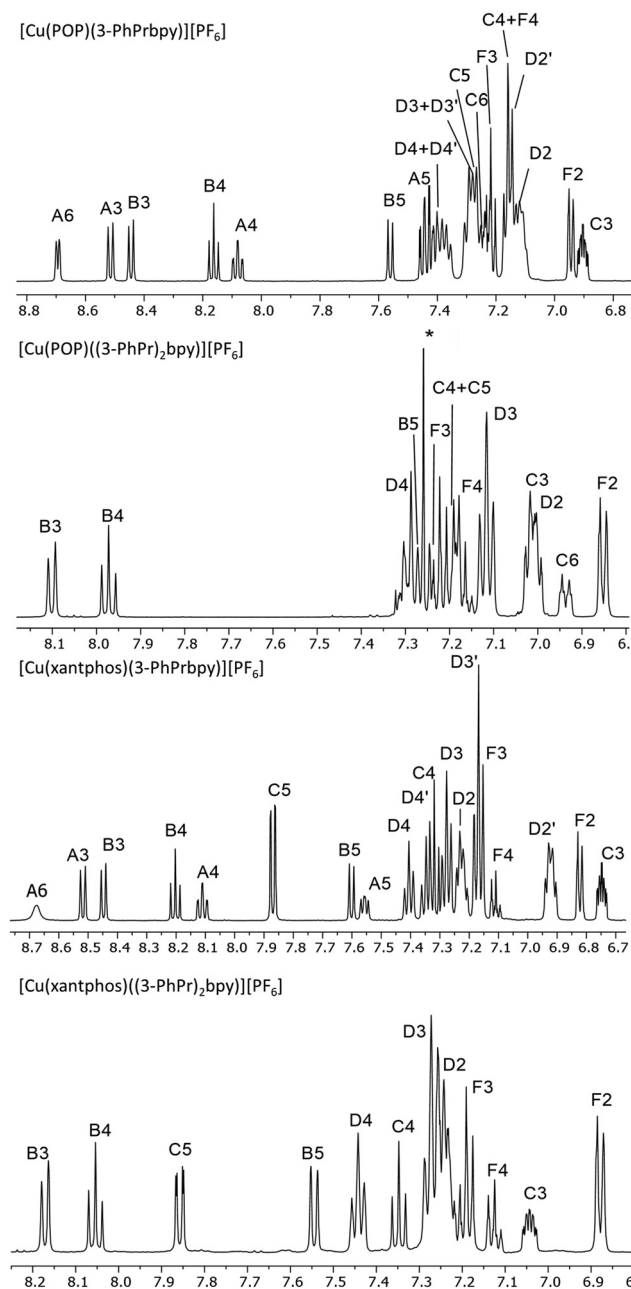


Fig. 1 Aromatic region of the 500 MHz ^1H NMR spectra of $[\text{Cu}(\text{POP})(3)][\text{PF}_6]$, $[\text{Cu}(\text{xantphos})(3)][\text{PF}_6]$, and $[\text{Cu}(\text{xantphos})((3)_2\text{bpy})][\text{PF}_6]$ in acetone- d_6 and $[\text{Cu}(\text{POP})((3)_2\text{bpy})][\text{PF}_6]$ in CDCl_3 . Chemical shifts in δ/ppm ; * = residual CHCl_3 . Atom labels are defined in Scheme 2.

and $[\text{Cu}((2\text{-CyEt})_2\text{bpy})_2][\text{PF}_6]$ were grown by slow diffusion of Et_2O into CH_2Cl_2 solutions of the compounds.

Crystallographic data are summarized in Table S1,[†] and important angles and bond distances defining the copper(i) coordination sphere are summarized in Table 1 together with published data for the benchmark compounds $[\text{Cu}(\text{POP})(\text{bpy})][\text{PF}_6]\cdot\text{CHCl}_3$ ³⁷ and $[\text{Cu}(\text{xantphos})(\text{bpy})][\text{PF}_6]$ ³⁸ for comparison. The molecular structures of the complex cations are shown in Fig. S128–S140.[†] Most of the complexes crystallized

in the triclinic space group $P\bar{1}$ with exceptions being $[\text{Cu}(\text{POP})(3\text{-EtPentbpy})][\text{PF}_6]$ (polymorph 1) (monoclinic $P2_1/n$), $[\text{Cu}(\text{POP})(3\text{-PhPrbpy})][\text{PF}_6]$ (monoclinic $P2_1/n$), $[\text{Cu}(\text{xantphos})(2\text{-PhEtbpy})][\text{PF}_6]$ (monoclinic $C2/c$) and $[\text{Cu}(\text{POP})(3\text{-EtPentbpy})][\text{PF}_6]\cdot 1.125\text{Et}_2\text{O}$ crystallized with two crystallographically independent ion-pairs. For the complex $[\text{Cu}(\text{POP})(3\text{-EtPentbpy})][\text{PF}_6]$, two different polymorphs were obtained, polymorph 1 being crystallized in the space group $P2_1/n$, whereas polymorph 2 crystallized in the space group $Pbca$. The two polymorphs were obtained from two crystals of two identically set up crystallization vessels (layer diffusion crystallization from CH_2Cl_2 solution with Et_2O).

For simplicity, the discussion below states the formulae of the coordination compounds without stating the solvents of crystallization. Important structural parameters for the structure of the homoleptic complex $[\text{Cu}((2\text{-CyEt})_2\text{bpy})_2][\text{PF}_6]$ are given in Table 1 and the structure of the cation is shown in Fig. S140.[†] The structures of the heteroleptic complex cations exhibit the expected bidentate chelating mode of both the bisphosphane and diimine ligands (Fig. 2a). In each structure, the copper(i) centre exhibits a distorted tetrahedral coordination geometry. The angles between the NCuN plane and the PCuP plane range from 90° in $[\text{Cu}(\text{POP})((2\text{-PhEt})_2\text{bpy})][\text{PF}_6]$ (molecule 2, Table 1) to 78.6° in $[\text{Cu}(\text{xantphos})((2\text{-PhEt})_2\text{bpy})][\text{PF}_6]$ (Table 1). A number of complexes in the series exhibit greater degrees of distortion than in related $[\text{Cu}(\text{POP})(\text{N}^+\text{N})]^+$ or $[\text{Cu}(\text{xantphos})(\text{N}^+\text{N})]^+$ cations reported previously.³⁹ This can be attributed to the increased strain on the coordination sphere exerted by the sterically demanding substituents present in this series. However, there is no correlation between the angle between the NCuN and PCuP planes and the dihedral N-C-C-N torsion angle of the bpy ligand (Table 1, last 2 columns). The P-Cu-P chelating angles vary considerably from $111.62(2)^\circ$ in $[\text{Cu}(\text{POP})(3\text{-EtPentbpy})][\text{PF}_6]$ to $119.54(2)^\circ$ in $[\text{Cu}(\text{xantphos})((2\text{-PhEt})_2\text{bpy})][\text{PF}_6]$. This range is comparable with values found for related complexes.³⁹ The Cu-N and Cu-P distances all lie within a typical range of $2.028(4)$ to $2.162(2)$ Å and $2.230(2)$ to $2.325(2)$ Å, respectively.

In all xantphos-containing compounds, the sterically more demanding substituent on the bpy ligand is accommodated in the ‘bowl-shaped’ xanthene unit of the P^+P ligand (Fig. 2b and 3). In addition, the embrace of the bulky substituents in the four crystal structures of the disubstituted complexes $[\text{Cu}(\text{POP})((2\text{-PhEt})_2\text{bpy})]^+$, $[\text{Cu}(\text{xantphos})((2\text{-PhEt})_2\text{bpy})]^+$, $[\text{Cu}(\text{POP})((3\text{-PhPr})_2\text{bpy})]^+$ and $[\text{Cu}(\text{xantphos})(6\text{-Cy-6'-Mebpy})]^+$ (see Fig. S134, S135, S138 and S139[†]) indicates how the added moieties in this series can aid to protect the metal centre. Most of the xantphos-containing crystal structures exhibit offset face-to-face π stacking interactions between phenyl rings of each of the two different PPh_2 units (Fig. 2c). The exceptions are $[\text{Cu}(\text{xantphos})((2\text{-PhEt})_2\text{bpy})][\text{PF}_6]$ (Fig. S135[†]) and $[\text{Cu}(\text{xantphos})(6\text{-Cy-6'-Mebpy})][\text{PF}_6]$ (Fig. S139[†]).

In $[\text{Cu}(\text{xantphos})(2\text{-CyEtbpy})][\text{PF}_6]$, the angle between the least squares planes containing the π -stacked phenyl rings is 4.7° , the average of the two centroid...plane distances is 3.73 Å

Table 1 Important structural parameters in the cations in [Cu(P[^]P)(N[^]N)][PF₆]. Benchmark [Cu(P[^]P)(bpy)][PF₆] complexes are included for comparison

Complex	P–Cu–P chelating angle/°	N–Cu–N chelating angle/°	P...P distance/ Å	Angle between PCuP and NCuN planes/°	N–C–C–N torsion angle/°
[Cu(POP)(bpy)][PF ₆] ^a	115.00(3)	79.66(7)	3.790(1)	88.5	–2.8(3)
[Cu(xantphos)(bpy)][PF ₆] ^b	113.816(14)	79.32(5)	3.8010(5)	79.6	20.5(2)
[Cu(xantphos)(2-CyEtbp)] [PF ₆]	113.52(6)	80.2(2)	3.797(2)	89.9	–0.9(8)
[Cu(POP)(3-EtPentbp)] [PF ₆] (poly- morph 1)	111.62(2)	79.90(7)	3.7605(8)	85.7	7.4(3)
[Cu(POP)(3-EtPentbp)] [PF ₆] (poly- morph 2)	113.21(3)	79.50(9)	3.7770(9)	85.5	5.8(4)
[Cu(xantphos)(3-EtPentbp)] [PF ₆]	113.29(3)	80.27(12)	3.791(1)	88.8	0.1(5)
[Cu(POP)(2-PhEtbp)] [PF ₆]	113.34(4)	80.35(12)	3.791(1)	88.7	2.9(5)
[Cu(xantphos)(2-PhEtbp)] [PF ₆]	113.86(3)	79.78(11)	3.802(1)	89.9	–10.2(4)
[Cu(POP)((2-PhEt) ₂ bpy)] [PF ₆] mole- cule 1 ^c	116.91(6)	81.4(2)	3.874(2)	88.9	–7.9(9)
[Cu(POP)((2-PhEt) ₂ bpy)] [PF ₆] mole- cule 2 ^c	118.00(6)	80.70(19)	3.906(2)	90.0	1.1(8)
[Cu(xantphos)((2-PhEt) ₂ bpy)] [PF ₆]	119.54(2)	80.74(7)	3.9255(7)	78.6	27.7(3)
[Cu(POP)(3-PhPrbp)] [PF ₆]	111.82(5)	80.10(15)	3.760(2)	87.1	9.3(6)
[Cu(xantphos)(3-PhPrbp)] [PF ₆]	112.81(5)	79.93(17)	3.776(2)	89.7	–0.4(6)
[Cu(POP)((3-PhPr) ₂ bpy)] [PF ₆]	114.427(15)	79.82(5)	3.8331(6)	89.7	–12.1(2)
[Cu(xantphos)(6-Cy-6'-Mebpy)] [PF ₆]	119.35(2)	79.80(8)	3.9518(7)	88.6	10.0(3)
[Cu((2-CyEt) ₂ bpy) ₂][PF ₆]	—	81.77(13) (N1, N2); 81.47(13) (N3, N4)	—	89.6 (two NCuN planes)	–7.9(5) (N1, N2); 4.8(5) (N3, N4)

^a Data for [Cu(POP)(bpy)][PF₆].CHCl₃ (CSD refcode OYUKID).³⁷ ^b Data for [Cu(xantphos)(bpy)][PF₆] (CSD refcode VICRAD).³⁸ ^c Two crystallographically independent ion-pairs.

and the centroid...centroid distance is 3.79 Å. These parameters are 3.9°, 3.7 and 3.8 Å for [Cu(xantphos)(3-EtPentbp)] [PF₆], 4.5°, 3.6 Å and 3.8 Å for [Cu(xantphos)(2-PhEtbp)] [PF₆] and 3.2°, 3.7 Å and 3.8 Å for [Cu(xantphos)(3-PhPrbp)] [PF₆]. These all comply with the definitions delineated by Janiak.⁴⁰ In [Cu(xantphos)(6-Cy-6'-Mebpy)] [PF₆], the face-to-face π -stacking is inhibited by the highly sterically demanding 6-Cy-6'-Mebpy ligand where the methyl substituent is forced between the two respective phenyl rings, causing them to lie at an angle of 51.4° with respect to one other. Fig. 2j illustrates the significant steric hindrance exerted by the 6-Cy-6'-Mebpy ligand, and this is substantiated in Fig. 3f.

In [Cu(xantphos)((2-PhEt)₂bpy)] [PF₆], two phenyl rings of each PPh₂ unit exhibit C–H... π -contacts as shown in Fig. 2d, thus contrasting with the face-to-face π -stacking discussed for the other xantphos-containing complexes. In addition, the PPh₂-phenyl ring containing C61 (see Fig. S135†) is involved in a C–H... π -contact with the bpy-backbone arene ring containing N1 analogous to the illustration in Fig. 2h. The same kind of C–H... π interaction is exhibited at least once in each of the structures with the exception of [Cu(xantphos)(2-PhEtbp)] [PF₆] where the C–H... π interaction is directed at the centroid of the Cu(N[^]N) chelate. The C–H...centroid distances lie in the range 2.61 to 3.82 Å. These interactions are in agreement with the contact definitions by Nishio.⁴¹

In both crystallographically independent molecules of [Cu(POP)((2-PhEt)₂bpy)] [PF₆], a phenyl ring from one PPh₂-unit shows an offset π -stacking interaction over the bpy domain (Fig. 2e). A rather similar interaction occurs in [Cu(xantphos)((2-PhEt)₂bpy)] [PF₆] (Fig. 2f), but here the interaction involves

only one of the pyridine rings of the bpy domain. The angle between the least squares planes containing the π -stacked phenyl rings is 12.5°, and the centroid...centroid distance is 3.78 Å.

In [Cu(POP)(3-EtPentbp)] [PF₆] (polymorph 1), one phenyl ring of the PPh₂ unit engages in a π -stacking contact with one phenyl ring of the POP-backbone. The angle between the least squares planes of the rings is 26.7°, and the centroid...centroid distance is 4.09 Å. For the other structures exhibiting this feature, the corresponding parameters are 19.0° and 3.87 Å in [Cu(POP)(2-PhEtbp)] [PF₆], and 13.5° and 3.71 Å in [Cu(POP)(3-PhPrbp)] [PF₆]. A feature which is present in all but two crystal structures of POP-containing complexes is an embrace comprising C–H... π contacts between two phenyl rings of a PPh₂ unit and the neighbouring POP backbone arene ring (Fig. 2i).

Electrochemistry

Cyclic voltammetry was used to investigate the redox properties of the complexes in solutions of dry 4-methyl-1,3-dioxolan-2-one containing 0.1 mol dm^{–3} [nBu₄N][PF₆] as supporting electrolyte. The cyclic voltammograms of the complexes are presented in Fig. S141 and S142.† Potentials were referenced internally to ferrocene. In each cyclic voltammogram (CV), the Cu⁺/Cu²⁺ oxidation appears between E_{pa} = +0.85 and +0.98 V (Table 2) and is typically irreversible. For all the complexes, a partially reversible reduction with $E_{1/2}^{red}$ values ranging from –2.13 to –2.02 V was observed. Assuming an orbital localization and distribution similar to those in previously reported



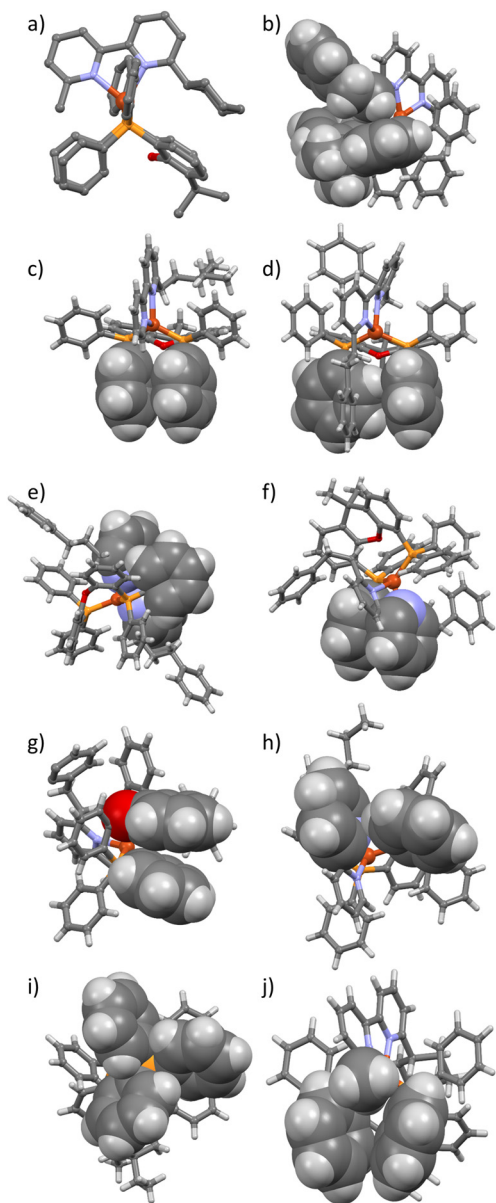


Fig. 2 Selected structural features of the $[\text{Cu}(\text{P}^{\wedge}\text{P})(\text{N}^{\wedge}\text{N})]^+$ cations: (a) perspective along the P–P vector perpendicular to the 6-Cy-6'-Mebpy-plane in $[\text{Cu}(\text{xantphos})(6\text{-Cy-6'-Mebpy})][\text{PF}_6]$ (H-atoms omitted for clarity); (b) accommodation of the 2-phenylethyl substituent of 2-PhEtbp within the xanthene 'cavity' in $[\text{Cu}(\text{xantphos})(2\text{-PhEtbp})][\text{PF}_6]$; (c) face-to-face π -stacking of two phenyl rings connected to the two different PPh_2 units in $[\text{Cu}(\text{xantphos})(3\text{-EtPentbp})][\text{PF}_6]$; (d) C–H... π interaction of two phenyl rings connected to the two different PPh_2 units in $[\text{Cu}(\text{xantphos})((2\text{-PhEt})_2\text{bpy})][\text{PF}_6]$; (e) offset π -stacking of one POP-phenyl ring with the (3-PhPr) $_2$ bpy ligand in $[\text{Cu}(\text{POP})((3\text{-PhPr})_2\text{bpy})][\text{PF}_6]$; (f) face-to-face π -stacking one PPh_2 -phenyl ring and one bpy-backbone ring in $[\text{Cu}(\text{xantphos})((2\text{-PhEt})_2\text{bpy})][\text{PF}_6]$; (g) face-to-face π -stacking of one POP-phenyl ring with a POP backbone ring in $[\text{Cu}(\text{POP})(2\text{-PhEtbp})][\text{PF}_6]$; (h) C–H... π interaction between one PPh_2 unit phenyl ring and one bpy-backbone ring in $[\text{Cu}(\text{POP})(3\text{-EtPentbp})][\text{PF}_6]$; (i) C–H... π contacts between two phenyl rings of a PPh_2 unit and the neighbouring POP backbone ring in $[\text{Cu}(\text{POP})(3\text{-EtPentbp})][\text{PF}_6]$; (j) accommodation of the methyl substituent of the 6-Cy-6'-Mebpy ligand in $[\text{Cu}(\text{xantphos})(6\text{-Cy-6'-Mebpy})][\text{PF}_6]$. The cyclohexyl group lies in the xanthene 'bowl' as depicted in Fig. 3f, illustrating the steric demand of the $\text{N}^{\wedge}\text{N}$ -ligand.

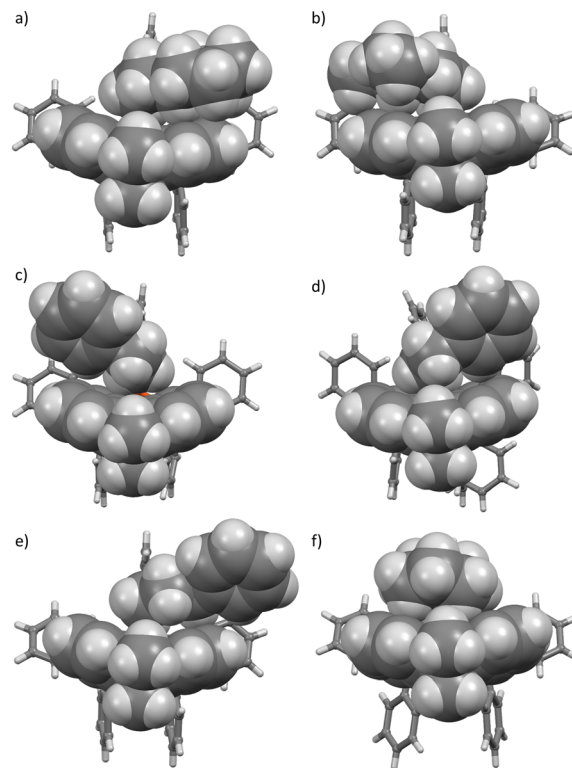


Fig. 3 Accommodation of sterically demanding substituents attached to the $\text{N}^{\wedge}\text{N}$ ligand within the 'bowl-shaped' xanthene unit. The aliphatic linker reaches into the centre of the 'bowl' with the more bulky moieties folding away from the xanthene unit. (a) 2-cyclohexyl-ethyl-substituent in $[\text{Cu}(\text{xantphos})(2\text{-CyEtbp})][\text{PF}_6]$; (b) 3-ethyl-pentyl-substituent in $[\text{Cu}(\text{xantphos})(3\text{-EtPentbp})][\text{PF}_6]$; (c) 2-phenyl-ethyl-substituent in $[\text{Cu}(\text{xantphos})(2\text{-PhEtbp})][\text{PF}_6]$; (d) one 2-phenyl-ethyl-substituent in $[\text{Cu}(\text{xantphos})((2\text{-PhEt})_2\text{bpy})][\text{PF}_6]$; (e) 3-phenyl-propyl-substituent in $[\text{Cu}(\text{xantphos})(3\text{-PhPrbp})][\text{PF}_6]$; (f) cyclohexyl-substituent in $[\text{Cu}(\text{xantphos})(6\text{-Cy-6'-Mebpy})][\text{PF}_6]$.

complexes,^{18,37,38} this reduction process is centred on the $\text{N}^{\wedge}\text{N}$ ligand.

Oxidation of the copper(i) centre is accompanied by flattening of the coordination sphere since copper(ii) prefers a square-planar environment. We expect that introducing bulky substituents will push the oxidation process to higher potentials. This has already been observed for a series of related compounds: the E_{pa} values for $[\text{Cu}(\text{xantphos})(\text{Me}_2\text{bpy})][\text{PF}_6]$ ($E_{\text{pa}} = +0.91$ V) and $[\text{Cu}(\text{POP})(\text{Me}_2\text{bpy})][\text{PF}_6]$ ($E_{\text{pa}} = +0.93$ V)³⁹ are higher than those for $[\text{Cu}(\text{xantphos})(\text{bpy})][\text{PF}_6]$ and $[\text{Cu}(\text{POP})(\text{bpy})][\text{PF}_6]$ (+0.87 and +0.83 V, respectively).³⁸ Inspection of the data in Table 2 reveals that the $\text{Cu}^+/\text{Cu}^{2+}$ oxidation processes in the present series of compounds tend to lie at a higher potentials than for $[\text{Cu}(\text{xantphos})(\text{Me}_2\text{bpy})][\text{PF}_6]$ and $[\text{Cu}(\text{POP})(\text{Me}_2\text{bpy})][\text{PF}_6]$. When comparing the POP-containing with the xantphos-containing complexes, a general trend is observed that the $\text{Cu}^+/\text{Cu}^{2+}$ oxidation of the xantphos complexes occurs at a higher potential. Only the two complexes $[\text{Cu}(\text{POP})((2\text{-PhEt})_2\text{bpy})][\text{PF}_6]$ and $[\text{Cu}(\text{xantphos})((2\text{-PhEt})_2\text{bpy})][\text{PF}_6]$ deviate from this trend. In these two complexes, the $\text{N}^{\wedge}\text{N}$ ligand is to be expected to exert a particularly



Table 2 Cyclic voltammetric data for [Cu(P[^]P)(N[^]N)][PF₆] in 4-methyl-1,3-dioxolan-2-one (10^{−4} to 10^{−5} mol dm^{−3}, vs. Fc/Fc⁺, [t[^]Bu₄N][PF₆] as supporting electrolyte, scan rate = 0.1 V s^{−1}). For irreversible oxidative processes, only (i) E_{pa} is given

Complex	Oxidative process E _{pa} /V	Reductive process	
		E _{1/2} ^{red} /V	E _{pa} − E _{pc} /mV
[Cu(POP)(2-CyEtbpv)][PF ₆]	+0.85	−2.07	80
[Cu(xantphos)(2-CyEtbpv)][PF ₆]	+0.93	−2.06	80
[Cu(POP)(3-EtPentbpv)][PF ₆]	+0.85	−2.09	90
[Cu(xantphos)(3-EtPentbpv)][PF ₆]	+0.97	−2.06	70
[Cu(POP)(2-PhEtbpv)][PF ₆]	+0.85	−2.09	60
[Cu(xantphos)(2-PhEtbpv)][PF ₆]	+0.93	−2.05	60
[Cu(POP)((2-PhEt) ₂ bpy)][PF ₆]	+0.98	−2.07	90
[Cu(xantphos)((2-PhEt) ₂ bpy)][PF ₆]	+0.92	−2.07	70
[Cu(POP)(3-PhPrbpv)][PF ₆]	+0.86	−2.05	60
[Cu(xantphos)(3-PhPrbpv)][PF ₆]	+0.96	−2.02	60
[Cu(POP)((3-PhPr) ₂ bpy)][PF ₆]	+0.94	−2.10	70
[Cu(xantphos)((3-PhPr) ₂ bpy)][PF ₆]	+0.97	−2.11	70
[Cu(xantphos)(6-Cy-6'-Mebpy)][PF ₆]	+0.97	−2.11	60

strong restraining effect for the tetrahedral coordination geometry. This effect seems to be even stronger with the groups introduced in this series compared to the effect of one or two methyl groups.³⁹ This finding is affirmed by the complexes reported by Wöhler *et al.*⁴

Photophysical properties

The solution absorption spectra of the complexes exhibit intense high-energy absorption bands below *ca.* 330 nm, originating from ligand-centred, spin-allowed $\pi^* \leftarrow \pi$ transitions. Additionally, each spectrum comprises a broad, lower-intensity MLCT band with λ_{max} in the ranges 369–384 nm for the POP-containing complexes and 369–382 nm for the xanthous-containing complexes. A blue-shift of *ca.* 10 nm is observed upon going from the MLCT absorption maxima of complexes containing the 6-substituted bpy ligands (avg. 381 nm, std. dev. 1.5 nm) to the MLCT absorption maxima of the complexes containing the 6,6'-disubstituted bpy ligands (avg. 371 nm, std. dev. 2.9 nm). This observation is analogous to the comparison of the MLCT bands between the Mebpy- and Me₂bpy-containing complexes discussed previously.³⁹ This can be accounted for by the electron-donating character of the alkyl substituents, which destabilizes the LUMO to a greater extent in the disubstituted bpy containing complexes. The absorption spectra are displayed in Fig. 4 and 5 and the absorption data are given in Table 3.

The normalized solution emission spectra of the complexes in deaerated CH₂Cl₂ with an excitation wavelength in the region of their MLCT bands are displayed in Fig. 6 and 7. The complexes' solid-state (powder) emission spectra are shown in Fig. 8 and 9. In related heteroleptic [Cu(P[^]P)(N[^]N)]⁺ complexes,¹⁸ the emissions have been assigned to $\pi^*(\text{bpy}) \leftarrow d\pi(\text{Cu})$ (³MLCT) transitions. All emission-related photophysical data are summarized in Table 4. Solution emission spectra were measured with an excitation wavelength of $\lambda_{\text{exc}} = 410$ nm to avoid overlapping of the second harmonic of the excitation peak with the broad emission band. Excitation at $\lambda_{\text{exc}} = 365$ nm resulted in an identical emission band after normalization.

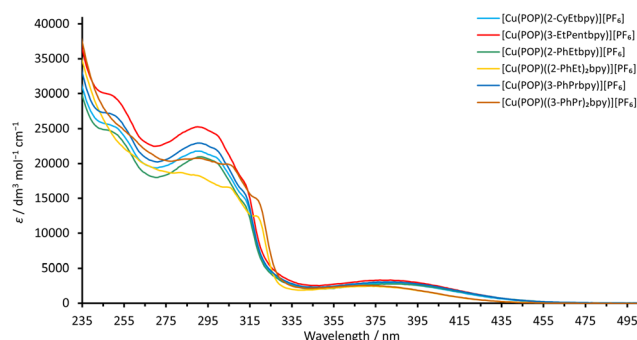


Fig. 4 Solution absorption spectra (CH₂Cl₂, 2.5 × 10^{−5} mol dm^{−3}) of the POP-containing heteroleptic copper(I) complexes.

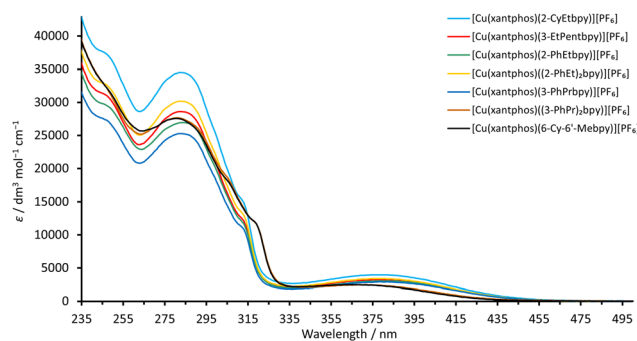


Fig. 5 Solution absorption spectra (CH₂Cl₂, 2.5 × 10^{−5} mol dm^{−3}) of the xantphos-containing heteroleptic copper(I) complexes.

In solution, the emission maxima are red-shifted with respect to the respective solid-state emission bands to a range between 564 and 635 nm. This corresponds to a yellow or orange solution photoluminescence (PL). The red shift agrees with previous observations for related families of complexes.¹⁸ While staying either in the POP- or xantphos-subgroup of the series, upon changing from complexes containing a 6-substituted bpy to a 6,6'-disubstituted bpy ligand, the solution emission maxima are



Table 3 Absorption maxima for CH₂Cl₂ solutions of [Cu(P[^])(N[^]N)][PF₆]

Complex	$\lambda_{\text{max}}^a/\text{nm}$ ($\epsilon_{\text{max}}/\text{dm}^3 \text{ mol}^{-1} \text{ cm}^{-1}$)	MLCT
[Cu(POP)(2-CyEtbpv)][PF ₆]	$\pi^* \leftarrow \pi$ 250 (25 500), 290 (21 900), 300 (20 700), 305 sh (18 400), 314 sh (14 000)	380 (2780)
[Cu(xantphos)(2-CyEtbpv)][PF ₆]	247 (36 900), 284 (34 100), 300 sh (24 400), 313 sh (14 700)	380 (3950)
[Cu(POP)(3-EtPentbpv)][PF ₆]	251 (29 400), 293 (25 100), 312 sh (17 500)	381 (3300)
[Cu(xantphos)(3-EtPentbpv)][PF ₆]	248 (31 300), 284 (29 000), 301 sh (19 900), 313 sh (12 300)	380 (3290)
[Cu(POP)(2-PhEtbpv)][PF ₆]	250 (24 500), 292 (20 900), 300 (19 800), 314 sh (13 100)	382 (2680)
[Cu(xantphos)(2-PhEtbpv)][PF ₆]	249 (30 200), 275 (26 800), 299 (21 200), 313 sh (12 100)	382 (3140)
[Cu(POP)((2-PhEt) ₂ bpy)][PF ₆]	260 sh (31 300), 282 (18 900), 290 (18 500), 305 (16 900), 313 sh (12 700)	369 (2460)
[Cu(xantphos)((2-PhEt) ₂ bpy)][PF ₆]	246 sh (32 900), 283 (30 200), 289 (29 400), 299 (22 500), 312 sh (13 400)	376 (3440)
[Cu(POP)(3-PhPrbpy)][PF ₆]	249 (27 400), 284 (22 500), 290 (23 200), 298 (22 300), 305 (19 400), 312 sh (16 100)	382 (3080)
[Cu(xantphos)(3-PhPrbpy)][PF ₆]	248 (27 100), 277 (24 700), 282 (25 300), 288 (24 900), 298 (19 300), 311 sh (11 400)	379 (3820)
[Cu(POP)((3-PhPr) ₂ bpy)][PF ₆]	255 sh (24 500), 287 (20 600), 305 (19 400), 318 sh (14 600)	369 (2480)
[Cu(xantphos)((3-PhPr) ₂ bpy)][PF ₆]	246 sh (32 900), 280 (27 800), 290 (26 600), 307 sh (17 800), 320 sh (11 200)	371 (2540)
[Cu(xantphos)(6-Cy-6'-Mebpy)][PF ₆]	247 sh (31 800), 281 (37 500), 291 (25 200), 305 sh (18 200), 320 sh (11 000)	370 (2200)

^a Solution concentration = $2.5 \times 10^{-5} \text{ mol dm}^{-3}$; sh = shoulder

significantly blue-shifted by *ca.* 55–60 nm. This is explained both by the increased steric stabilization of the coordination sphere and the increased destabilization of the LUMO through the σ -electron-donating character of the alkyl substituents. The finding is also reinforced by the comparison between the Mebpv and Me₂bpy containing complexes reported earlier.³⁹

All the copper(i) complexes are green to yellow PL emitters in powdered form. The solid-state emission maxima of the POP-containing compounds lie between 555 and 567 nm with two outliers at 518 nm ([Cu(POP)((3-PhPr)₂bpy)][PF₆]) and 526 nm ([Cu(POP)(2-PhEtbpv)][PF₆]). The solid-state emission maxima of the xantphos-containing complexes lie at lower

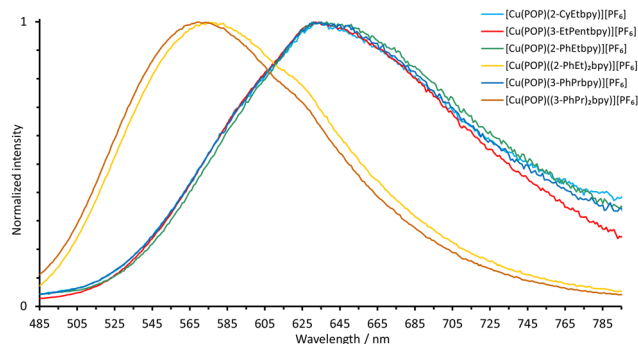


Fig. 6 Normalized solution emission spectra of the POP-containing heteroleptic copper(i) complexes (deaerated CH₂Cl₂, $1.0 \times 10^{-5} \text{ mol dm}^{-3}$, $\lambda_{\text{exc}} = 365 \text{ nm}$).

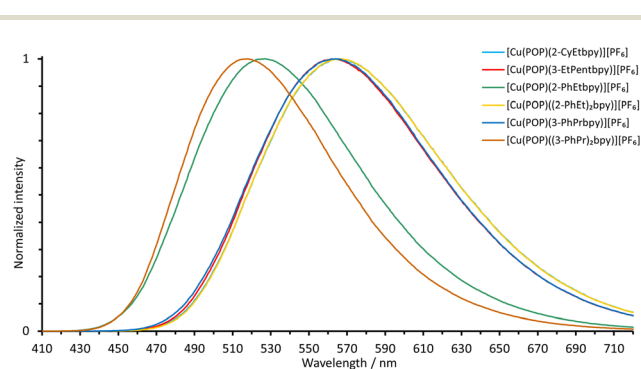


Fig. 8 Normalized emission spectra of powdered samples of the POP-containing heteroleptic copper(i) complexes ($\lambda_{\text{exc}} = 365 \text{ nm}$).

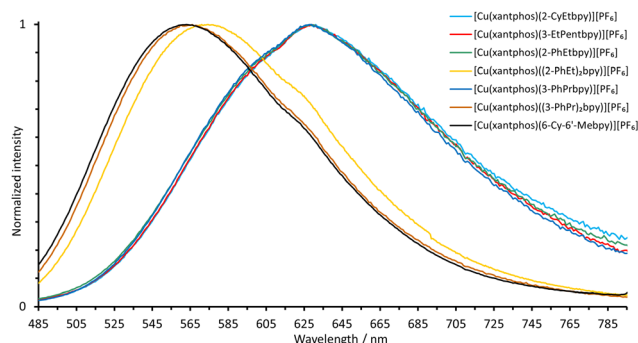


Fig. 7 Normalized solution emission spectra of the xantphos-containing heteroleptic copper(i) complexes (deaerated CH₂Cl₂, $1.0 \times 10^{-5} \text{ mol dm}^{-3}$, $\lambda_{\text{exc}} = 365 \text{ nm}$).

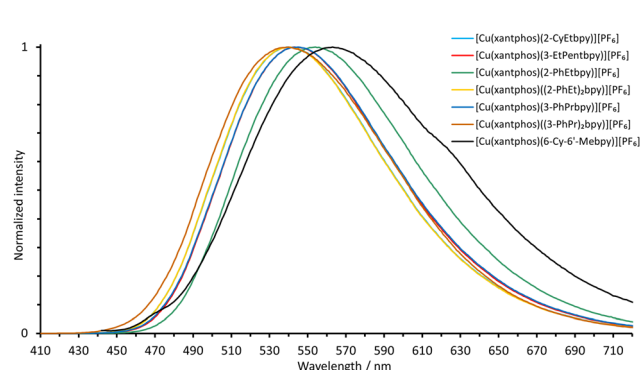


Fig. 9 Normalized emission spectra of powdered samples of the xantphos-containing heteroleptic copper(i) complexes ($\lambda_{\text{exc}} = 365 \text{ nm}$).

Table 4 Photophysical properties of the [Cu(P[^]P)(N[^]N)][PF₆] complexes

Complex	Solution ^a			Powder ^c				
	$\lambda_{\text{max}}^{\text{em}}/ \text{nm}$	PLQY ^c /%	$\tau^c/\mu\text{s}$	$\lambda_{\text{max}}^{\text{em}}/\text{nm}$	PLQY/%	$\langle\tau\rangle^d/\mu\text{s}$	$\tau(1)/\mu\text{s}$ (A_1)	$\tau(2)/\mu\text{s}$ (A_2)
[Cu(POP)(2-CyEtbp)] [PF ₆]	634	0.9	0.31	567	11	4.0	5.5 (0.55)	1.9 (0.40)
[Cu(xantphos)(2-CyEtbp)] [PF ₆]	628	1.4	0.68	542	26	9.1	10.1 (0.83)	2.4 (0.13)
[Cu(POP)(3-EtPentbp)] [PF ₆]	634	0.9	0.30	563	14	5.1	5.5 (0.88)	1.7 (0.087)
[Cu(xantphos)(3-EtPentbp)] [PF ₆]	629	1.4	0.68	543	24	8.8	9.8 (0.83)	2.3 (0.13)
[Cu(POP)(2-PhEtbp)] [PF ₆]	636	0.9	0.29	526	36	10.9	11.6 (0.89)	2.2 (0.072)
[Cu(xantphos)(2-PhEtbp)] [PF ₆]	628	1.1	0.76	554	20	7.5	8.4 (0.80)	2.5 (0.14)
[Cu(POP)((2-PhEt) ₂ bpy)] [PF ₆]	583, 626	10.7	3.8	567	67	4.0	5.4 (0.56)	1.9 (0.38)
[Cu(xantphos)((2-PhEt) ₂ bpy)] [PF ₆]	578, 628	1.5	0.63	541	27	9.1	10.2 (0.82)	2.3 (0.13)
[Cu(POP)(3-PhPrbp)] [PF ₆]	635	0.9	0.31	564	14	4.8	5.4 (0.79)	2.2 (0.16)
[Cu(xantphos)(3-PhPrbp)] [PF ₆]	629	1.6	0.78	545	23	6.5	7.5 (0.77)	2.1 (0.18)
[Cu(POP)((3-PhPr) ₂ bpy)] [PF ₆]	570, 616	21.2	5.2	518	72	14.1	14.6 (0.92)	1.3 (0.033)
[Cu(xantphos)((3-PhPr) ₂ bpy)] [PF ₆]	566, 616	18.0	4.8	540	18	6.8	8.9 (0.63)	1.9 (0.27)
[Cu(xantphos)(6-Cy-6'-Mebpy)] [PF ₆]	564, 614	14.9	3.9	563, 616	29	11.2	14.3 (0.68)	2.4 (0.24)

^a Deaerated, solution concentration = 1.0×10^{-5} mol dm⁻³. ^b excitation wavelength $\lambda_{\text{exc}} = 410$ nm. ^c excitation wavelength $\lambda_{\text{exc}} = 365$ nm. ^d A biexponential fit to the lifetime delay was used because a single exponential gave a poor fit; $\langle\tau\rangle$ is calculated from the equation $\sum A_i \tau_i / \sum (A_i)$ and A_i is the pre-exponential factor for the lifetime. Values of $\tau(1)$, $\tau(2)$, A_1 and A_2 are given as used for the calculation of $\langle\tau\rangle$. Deaeration was performed by bubbling a stream of argon through the solution.

wavelengths ($\lambda_{\text{max}}^{\text{em}} = 540$ to 554 nm) with the exception of [Cu(xantphos)(6-Cy-6'-Mebpy)][PF₆] which is red-shifted (Fig. 9 and Table 4). This complex has two emission bands, $\lambda_{\text{max}}^{\text{em}} = 563$ nm with a shoulder at 616 nm.

The appearance and luminescence of powdered samples of the [Cu(xantphos)(N[^]N)][PF₆] and [Cu(POP)(N[^]N)][PF₆] complexes are illustrated in Fig. 10 and S143,[†] respectively, with

samples shown under daylight and under UV irradiation ($\lambda_{\text{exc}} = 366$ nm).

The solid-state PLQY values (see Table 4) lie within the 11–72% range, whereas the solution values are notably lower (0.9–21%). For the complexes [Cu(P[^]P)(2-CyEtbp)][PF₆], [Cu(P[^]P)(3-EtPentbp)][PF₆] and [Cu(P[^]P)(3-PhPrbp)][PF₆], the xantphos-containing complexes have higher PLQY values compared to their POP-containing variants. In contrast, the complexes [Cu(POP)(2-PhEtbp)][PF₆], [Cu(POP)((2-PhEt)₂bpy)][PF₆] and [Cu(POP)((3-PhPr)₂bpy)][PF₆], have higher PLQYs than their xantphos counterparts.

The photophysical properties of the highest-performance compounds in this series exceed the values measured for the most promising complexes in the previously reported series. Switching from Mebp or Me₂bpy to more sterically demanding and longer chain substituents can thus be beneficial in achieving higher quantum yields, but caution is needed as this is not a general trend. The highest PLQY values were achieved with [Cu(POP)((2-PhEt)₂bpy)][PF₆] and [Cu(POP)((3-PhPr)₂bpy)][PF₆] both in the solid state and in solution. In deaerated solutions, the PLQY of [Cu(xantphos)((3-PhPr)₂bpy)][PF₆] as well as [Cu(xantphos)(6-Cy-6'-Mebpy)][PF₆] are also high. This underlines the fact that the 6,6'-disubstituted bpy ligands give rise to the strongest PL properties in the complexes. This is similar to previous findings³⁹ in which longer chain substituents seem to increase the PLQY values in solution and the solid state. The effect is however not always observed and it can be concluded, that the photophysical properties of the compounds rely on multiple factors. This renders any prediction difficult. For example, Linfoot *et al.* have previously presented the influence of different sample morphologies on the luminescence properties of the compound.⁴²

The copper(i) centres in the complexes described in this investigation are sterically highly protected and thus much less accessible to, for example, solvent molecules. Exciton

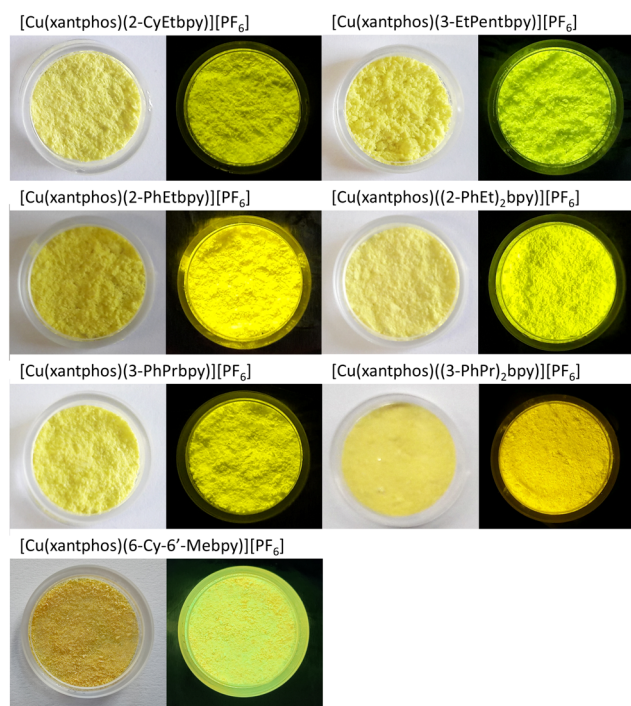


Fig. 10 Powder samples of [Cu(xantphos)(N[^]N)][PF₆] complexes, both under ambient light (left, white background) and under UV light ($\lambda_{\text{exc}} = 366$ nm, right, dark background).



quenching by non-radiative intermolecular processes such as collisional and static quenching,⁴³ Förster resonance energy transfer,⁴⁴ and Dexter electron transfer⁴⁵ are expected to be lowered. This makes this new series of complexes promising candidates for testing in a LEC environment.

The excited state lifetimes (τ) of the solid-state samples were determined using a bi-exponential fit;⁴⁶ the data for both solution and solid state are displayed in Table 4. The excited state lifetimes of the powder samples range from 4.0 μ s for [Cu(POP)(2-CyEtbp)] [PF₆] to 14.1 μ s for [Cu(POP)((3-PhPr)₂bpy)] [PF₆]. Between solutions of all salts, the majority of the 6,6'-disubstituted bpy-containing compounds ([Cu(POP)((2-PhEt)₂bpy)] [PF₆], [Cu(POP)((3-PhPr)₂bpy)] [PF₆], [Cu(xantphos)((3-PhPr)₂bpy)] [PF₆] and [Cu(xantphos)(6-Cy-6'-Mebpy)] [PF₆]) gave rise to increased excited state lifetimes compared to the 6-substituted bpy containing cations.

Conclusions

In this work, a series of bpy-based ligands with sterically demanding substituents in the 6- or 6,6'-positions was synthesized and characterized. Some of the ligands comprised phenyl rings connected *via* $-(CH_2)_n$ linkers to the bpy backbone to enable intramolecular π -interactions with arene rings in the P^P ligand in heteroleptic copper(i) complex cations. Complexes of the type [Cu(POP)(N^N)] [PF₆] and [Cu(xantphos)(N^N)] [PF₆] were prepared and characterized. The limits of steric hindrance were met with the ligands (2-CyEt)₂bpy, (3-EtPent)₂bpy, 4,4'-*t*Bu₂-6,6'-Cy₂bpy as demonstrated in the failed attempts to synthesize heteroleptic complexes containing these ligands. With the ligand 6-Cy-6'-Mebpy, only the heteroleptic complex containing xantphos could be isolated. This represents the only complex containing an asymmetric disubstituted ligand in the series. All complexes are green to yellow emitters in the solid state, and yellow or orange emitters in solution. The majority of the complexes were characterized by single-crystal X-ray diffraction and this confirmed the expected distorted tetrahedral copper(i) coordination environment. A feature in all the xantphos-containing complexes is the accommodation of the bulkier of the 6- and 6'-substituents of the bpy unit in the cavity of the xanthene unit of the P^P ligand. The complexes are redox active with typically irreversible Cu⁺/Cu²⁺ oxidation potentials lying between $E_{pa} = +0.85$ and $+0.98$ V. PLQY values in the solid state are in the range of 11–72%, whereas the deaerated solution values lie between 0.9–21%. As a general trend, the complexes prepared from 6,6'-disubstituted complexes with phenyl moieties connected *via* a CH₂CH₂ spacer have the highest values of PLQY. The most notable compounds are [Cu(POP)((2-PhEt)₂bpy)] [PF₆] (PLQY = 67%) and [Cu(POP)((3-PhPr)₂bpy)] [PF₆] (PLQY = 72%). These values are among the highest reported for [Cu(P^P)(N^N)] [PF₆] compounds. The solid-state values lie in the range of the values reported previously by Wöhler *et al.*⁴ A similar value was previously measured by Brunner *et al.* for the complex

[Cu(POP)(4,4'-bis(4-fluorophenyl)-6,6'-dimethyl-2,2'-bipyridine)] [PF₆] with a solid-state PLQY of 74%.⁴⁷

As expected, the PLQY values measured in solution are lower than the solid-state values, but the solution PLQYs for [Cu(POP)((3-PhPr)₂bpy)] [PF₆], [Cu(xantphos)((3-PhPr)₂bpy)] [PF₆], [Cu(xantphos)(6-Cy-6'-Mebpy)] [PF₆] and [Cu(POP)((2-PhEt)₂bpy)] [PF₆] (21.2, 18.0, 14.9 and 10.7%, respectively) are remarkable.

We conclude that the incorporation of more sterically demanding groups to the N^N ligands can be beneficial in terms of achieving higher quantum yields, but it is not generally an improvement in all cases. Especially the complexes prepared from symmetric bpy-derived ligands with phenyl rings connected *via* ethylene spacer in the 6,6'-position appear to have improved photophysical characteristics.

Note

This article is based upon part of a doctoral thesis entitled 'Synthesis and Characterization of Heteroleptic Copper(i) Complexes for Application in Light-Emitting Electrochemical Cells' (<https://edoc.unibas.ch/93771/>) written by Marco Meyer and supervised by Profs. Edwin C. Constable and Catherine E. Housecroft at the University of Basel.

Conflicts of interest

There are no conflicts to declare.

Acknowledgements

We thank the University of Basel for support.

References

- R. Czerwieniec, M. J. Leitl, H. H. H. Homeier and H. Yersin, *Coord. Chem. Rev.*, 2016, **325**, 2–28, DOI: [10.1016/j.ccr.2016.06.016](https://doi.org/10.1016/j.ccr.2016.06.016).
- H. Yersin, R. Czerwieniec, M. Z. Shafikov and A. F. Suleymanova, *ChemPhysChem*, 2017, **18**, 3508–3535, DOI: [10.1002/cphc.201700872](https://doi.org/10.1002/cphc.201700872).
- M. J. Leitl, D. M. Zink, A. Schinabeck, T. Baumann, D. Volz and H. Yersin, *Top. Curr. Chem.*, 2016, **374**, 25, DOI: [10.1007/s41061-016-0019-1](https://doi.org/10.1007/s41061-016-0019-1).
- J. Wöhler, M. Meyer, A. Prescimone, C. E. Housecroft and E. C. Constable, *Dalton Trans.*, 2022, **51**, 13094–13105, DOI: [10.1039/D2DT01799G](https://doi.org/10.1039/D2DT01799G).
- D. Gejsnæs-Schaad, M. Meyer, A. Prescimone, C. E. Housecroft and E. C. Constable, *CrystEngComm*, 2023, **25**, 3000–3012, DOI: [10.1039/D3CE00355H](https://doi.org/10.1039/D3CE00355H).
- C. E. Housecroft and E. C. Constable, *J. Mater. Chem. C*, 2022, 4456–4482, DOI: [10.1039/D1TC04028F](https://doi.org/10.1039/D1TC04028F).
- C. Sandoval-Pauker, M. Santander-Nelli and P. Dreyse, *RSC Adv.*, 2022, **12**, 10653–10674, DOI: [10.1039/D1RA08082B](https://doi.org/10.1039/D1RA08082B).



- 8 M. T. Buckner and D. R. McMillin, *J. Chem. Soc., Chem. Commun.*, 1978, 759–761, DOI: [10.1039/C39780000759](#).
- 9 R. A. Rader, D. R. McMillin, M. T. Buckner, T. G. Matthews, D. J. Casadonte, R. K. Lengel, S. B. Whittaker, L. M. Darmon and F. E. Lytle, *J. Am. Chem. Soc.*, 1981, **103**, 5906–5912, DOI: [10.1021/ja00409a048](#).
- 10 G. Blasse and D. R. McMillin, *Chem. Phys. Lett.*, 1980, **70**, 1–3, DOI: [10.1016/0009-2614\(80\)80047-9](#).
- 11 C. O. Dietrich-Buchecker, P. A. Marnot, J.-P. Sauvage, J. R. Kirchhoff and D. R. McMillin, *J. Chem. Soc., Chem. Commun.*, 1983, 513–515, DOI: [10.1039/C39830000513](#).
- 12 J. R. Kirchhoff, R. E. Gamache Jr., M. W. Blaskie, A. A. Del Paggio, R. K. Lengel and D. R. McMillin, *Inorg. Chem.*, 1983, **22**, 2380–2384, DOI: [10.1021/ic00159a008](#).
- 13 D. J. Casadonte Jr. and D. R. McMillin, *Inorg. Chem.*, 1987, **26**, 3950–3952, DOI: [10.1021/ic00270a025](#).
- 14 P. C. J. Kamer, P. W. N. M. van Leeuwen and J. N. H. Reek, *Acc. Chem. Res.*, 2001, **34**, 895–904, DOI: [10.1021/ar000060+](#).
- 15 E. Leoni, J. Mohanraj, M. Holler, M. Mohankumar, I. Nierengarten, F. Monti, A. Sournia-Saquet, B. Delavaux-Nicot, J.-F. Nierengarten and N. Armaroli, *Inorg. Chem.*, 2018, **57**, 15537–15549, DOI: [10.1021/acs.inorgchem.8b02879](#).
- 16 N. Armaroli, G. Accorsi, M. Holler, O. Moudam, J.-F. Nierengarten, Z. Zhou, R. T. Wegh and R. Welter, *Adv. Mater.*, 2006, **18**, 1313, DOI: [10.1002/adma.200690041](#).
- 17 M. K. Eggleston, D. R. McMillin, K. S. Koenig and A. J. Pallenberg, *Inorg. Chem.*, 1997, **36**, 172–176, DOI: [10.1021/ic960698a](#).
- 18 S. Keller, A. Pertegás, G. Longo, L. Martínez, J. Cerdá, J. M. Junquera-Hernández, A. Prescimone, E. C. Constable, C. E. Housecroft, E. Ortí and H. J. Bolink, *J. Mater. Chem. C*, 2016, **4**, 3857–3871, DOI: [10.1039/C5TC03725E](#).
- 19 S. Keller, E. C. Constable, C. E. Housecroft, M. Neuburger, A. Prescimone, G. Longo, A. Pertegás, M. Sessolo and H. J. Bolink, *Dalton Trans.*, 2014, **43**, 16593–16596, DOI: [10.1039/C4DT02847C](#).
- 20 M. Alkan-Zambada, S. Keller, L. Martínez-Sarti, A. Prescimone, J. M. Junquera-Hernández, E. C. Constable, H. J. Bolink, M. Sessolo, E. Ortí and C. E. Housecroft, *J. Mater. Chem. C*, 2018, **6**, 8460–8471, DOI: [10.1039/C8TC02882F](#).
- 21 M. D. Weber, M. Viciano-Chumillas, D. Armentano, J. Cano and R. D. Costa, *Dalton Trans.*, 2017, **46**, 6312–6323, DOI: [10.1039/C7DT00810D](#).
- 22 M. Alkan-Zambada, E. C. Constable and C. E. Housecroft, *Molecules*, 2020, **25**, 2647, DOI: [10.3390/molecules25112647](#).
- 23 S. Keller, M. Alkan-Zambada, A. Prescimone, E. C. Constable and C. E. Housecroft, *Crystals*, 2020, **10**, 255, DOI: [10.3390/cryst10040255](#).
- 24 M. Mohankumar, M. Holler, E. Meichsner, J.-F. Nierengarten, F. Niess, J.-P. Sauvage, B. Delavaux-Nicot, E. Leoni, F. Monti, J. M. Malicka, M. Cocchi, E. Bandini and N. Armaroli, *J. Am. Chem. Soc.*, 2018, **140**, 2336–2347, DOI: [10.1021/jacs.7b12671](#).
- 25 G. J. Kubas, B. Monzyk and A. L. Crumbliss, in *Inorg. Synth.*, 1979, vol. 19, pp. 90–92.
- 26 F. Brunner, A. Babaei, A. Pertegás, J. M. Junquera-Hernández, A. Prescimone, E. C. Constable, H. J. Bolink, M. Sessolo, E. Ortí and C. E. Housecroft, *Dalton Trans.*, 2019, **48**, 446–460, DOI: [10.1039/C8DT03827A](#).
- 27 S.-H. Kim and R. D. Rieke, *Tetrahedron*, 2010, **66**, 3135–3146, DOI: [10.1016/j.tet.2010.02.061](#).
- 28 K. Maeyama, C. Okumura and N. Yonezawa, *Synth. Commun.*, 2002, **32**, 3159–3167, DOI: [10.1081/SCC-120013727](#).
- 29 C.-Y. Huang, J. Li, W. Liu and C.-J. Li, *Chem. Sci.*, 2019, **10**, 5018–5024, DOI: [10.1039/C8SC05631E](#).
- 30 *Software for the Integration of CCD Detector System Bruker Analytical X-ray Systems*, Bruker axs, Madison, WI, (after 2013).
- 31 G. Sheldrick, *Acta Crystallogr.*, 2015, **A71**, 3–8, DOI: [10.1107/S2053273314026370](#).
- 32 O. V. Dolomanov, L. J. Bourhis, R. J. Gildea, J. A. K. Howard and H. Puschmann, *J. Appl. Crystallogr.*, 2009, **42**, 339–341, DOI: [10.1107/S0021889808042726](#).
- 33 G. Sheldrick, *Acta Crystallogr.*, 2015, **C71**, 3–8, DOI: [10.1107/S2053229614024218](#).
- 34 L. Palatinus and G. Chapuis, *J. Appl. Crystallogr.*, 2007, **40**, 786–790, DOI: [10.1107/S0021889807029238](#).
- 35 L. Palatinus, S. J. Prathapa and S. van Smaalen, *J. Appl. Crystallogr.*, 2012, **45**, 575–580, DOI: [10.1107/S0021889812016068](#).
- 36 C. F. Macrae, I. Sovago, S. J. Cottrell, P. T. A. Galek, P. McCabe, E. Pidcock, M. Platings, G. P. Shields, J. S. Stevens, M. Towler and P. A. Wood, *J. Appl. Crystallogr.*, 2020, **53**, 226–235, DOI: [10.1107/S1600576719014092](#).
- 37 R. D. Costa, D. Tordera, E. Ortí, H. J. Bolink, J. Schönle, S. Graber, C. E. Housecroft, E. C. Constable and J. A. Zampese, *J. Mater. Chem.*, 2011, **21**, 16108–16118, DOI: [10.1039/C1JM12607E](#).
- 38 S. Keller, F. Brunner, J. M. Junquera-Hernández, A. Pertegás, M.-G. La-Placa, A. Prescimone, E. C. Constable, H. J. Bolink, E. Ortí and C. E. Housecroft, *ChemPlusChem*, 2018, **83**, 217–229, DOI: [10.1002/cplu.201700501](#).
- 39 M. Meyer, L. Mardegan, D. Tordera, A. Prescimone, M. Sessolo, H. J. Bolink, E. C. Constable and C. E. Housecroft, *Dalton Trans.*, 2021, **50**, 17920–17934, DOI: [10.1039/D1DT03239A](#).
- 40 C. Janiak, *Dalton Trans.*, 2000, 3885–3896, DOI: [10.1039/B003010O](#).
- 41 M. Nishio, *CrystEngComm*, 2004, **6**, 130–158, DOI: [10.1039/B313104A](#).
- 42 C. L. Linfoot, M. J. Leidl, P. Richardson, A. F. Rausch, O. Chepelin, F. J. White, H. Yersin and N. Robertson, *Inorg. Chem.*, 2014, **53**, 10854–10861, DOI: [10.1021/ic500889s](#).
- 43 K. G. Fleming, in *Encyclopedia of Spectroscopy and Spectrometry*, ed. J. C. Lindon, G. E. Tranter and D. W. Koppenaal, Academic Press, Oxford, 3rd edn, 2017, pp. 647–653.
- 44 T. Förster, *Ann. Phys.*, 1948, **2**, 55–75, DOI: [10.1002/andp.19484370105](#).



- 45 D. L. Dexter, *J. Chem. Phys.*, 1953, **21**, 836–850, DOI: [10.1063/1.1699044](https://doi.org/10.1063/1.1699044).
- 46 T. Hofbeck, U. Monkowius and H. Yersin, *J. Am. Chem. Soc.*, 2015, **137**, 399–404, DOI: [10.1021/ja5109672](https://doi.org/10.1021/ja5109672).
- 47 F. Brunner, L. Martínez-Sarti, S. Keller, A. Pertegás, A. Prescimone, E. C. Constable, H. J. Bolink and C. E. Housecroft, *Dalton Trans.*, 2016, **45**, 15180–15192, DOI: [10.1039/C6DT02665F](https://doi.org/10.1039/C6DT02665F).

